J Appl Electrochem (2009) 39:583–591
DOI 10.1007/s10800-008-9696-y

ORIGINAL PAPER

Electrochemical behavior of AZ91D magnesium alloy in phosphate medium—part I. Effect of pH

Fakiha El-Taib Heakal · Amany Mohammed Fekry · Mohammed Ziad Fatayerji

Received: 3 March 2008 / Accepted: 15 October 2008 / Published online: 4 November 2008

Abstract The influence of pH on the corrosion behavior of Mg-based AZ91D alloy was investigated in a constant composition phosphate medium using various electrochemical techniques, complemented with surface analysis data. The studied solutions were 0.1 M H_3PO_4, NaH_2PO_4, Na_2HPO_4 and Na_3PO_4 having pH values of 1.8, 4.5, 9.1 and 11.8, respectively. Spontaneous passivation was substantiated from monitoring the continuous positive shift of the open circuit corrosion potential with both immersion time and solution pH. The impedance data indicated more improvement in the insulating properties of the corrosion products formed on the alloy surface with increase in pH. The electrolyte pH plays a determinant influence on surface film properties, as films formed in phosphate solutions with higher pH values are thicker, thus affording better protection for the alloy than those formed in acidic solutions. Good agreement was observed between the results obtained from electrochemical techniques and those from EDX and XRD examinations. The alloy is more susceptible to corrosion in acidic phosphate solutions than in the alkaline ones. Crystalline magnesium (Mg), magnesium hydride (MgH_2) and magnesium oxide (MgO) were found to be the main constituents of the surface film after holding for 2 h in the acidic phosphate medium.

F. El-Taib Heakal (✉) · A. Mohammed Fekry · M. Ziad Fatayerji
Chemistry Department, Faculty of Science, Cairo University, Giza 12613, Egypt
e-mail: fakihaheakal@yahoo.com

A. Mohammed Fekry
e-mail: hham4@hotmail.com

M. Ziad Fatayerji
e-mail: mzf2001@hotmail.com

Keywords AZ91D alloy · Phosphate medium · AC-impedance · Potentiodynamic · pH

1 Introduction

Pure magnesium metal is emerging as the lightest of all known structural metals for current, new and innovative applications [1]. The unwise use of magnesium in wet and salt-laden environments gives rise to its poor corrosion reputation [2]. To achieve better corrosion behavior and radical change in the metal properties, magnesium alloys have been used for their many advantages, such as light density, high strength-to-weight ratio, good mechanical properties and excellent castability. All, these have made magnesium alloys the most versatile and attractive metallic materials for a broad range of uses in commercial, industrial and aerospace applications.

One of the major problems limiting the uses of magnesium alloys is their susceptibility to corrosion in different media [3]. The corrosion resistance depends widely on film formation and surface-electrolyte interaction and it varies with the medium to which the alloy is exposed. The most successful magnesium–aluminum alloy is AZ91D, which contains in its microstructure the primary α-Mg matrix, α eutectic phase, β phase (the intermetallic $Mg_{17}Al_{12}$) distributed along the α grain boundaries and segregated AlMn phase precipitated inside grains. The eutectic α Mg adjunct to the β phase is Al richer than the primary α Mg [4].

In general, the resistance of magnesium alloys to atmospheric corrosion is less than that of aluminium alloys and is comparable to that of mild steel [5]. A clean unprotected magnesium alloy surface exposed to indoor or outdoor atmospheres free from salt will develop a grey film. It is the objective of this work to investigate the stability of the

naturally air-formed corrosion product on AZ91D alloy in aqueous phosphate solutions with various pH. Previous studies concerning the electrochemical performance of AZ91D alloy in phosphate electrolytes dealt mainly with producing a film by chemical [6] or electrochemical [7] oxidation to form protective coatings on AZ91D substrate. Zhou et al. [8] found that the phosphate conversion coating on AZ91D alloy has a thickness of about 10 μm and is composed of a complex phosphate containing magnesium and aluminum with an amorphous structure. The formation mechanism depends on a local pH increase due to hydrogen evolution. Zhao et al. [9] obtained a chromium-free conversion coating for AZ91D alloy by using a phosphate–permanganate solution. The conversion coatings are relatively uniform and continuous, with thickness from 7 to 10 μm. Niu et al. [10] succeeded in forming a zinc phosphate coating on AZ91D alloy with a typical phosphate microstructure having better corrosion resistance due to the presence of crystalline zinc in the coat.

In the present study electrochemical characterization of the tested system was carried out using open circuit potential (OCP), electrochemical impedance spectroscopy (EIS) and potentiodynamic techniques complemented by EDX and XRD analysis methods whenever needed. EIS is a technique that can simultaneously provide information on the corrosion mechanisms and quantitatively assesses the stability of spontaneously formed passive layers on the alloy surface.

2 Experimental details

The metallic material used was a die cast AZ91D magnesium alloy having a chemical composition in wt% of: 9.0 Al, 0.67 Zn, 0.33 Mn, 0.03 Cu, 0.01 Si, 0.005 Fe, 0.002 Ni, 0.0008 Be and balance magnesium. The sample was cut into coupons and molded into a glass tube with epoxy resin leaving only one side unsealed to serve as a working electrode with a surface area of 0.2 cm^2. The solutions were prepared using Na_3PO_4, Na_2HPO_4, NaH_2PO_4 and H_3PO_4 (Analar grade reagents) and triply distilled water. The surface of the test electrode was mechanical polishing with abrasive paper (400–1,000 grades), degreasing in acetone, rinsing with ethanol and drying in air. A conventional three-electrode electrolytic cell was used with a coiled platinum wire counter electrode placed in a separate compartment connected to the cell via a fritted glass disc and (Hg/Hg_2Cl_2) saturated calomel reference electrode (SCE). In the middle compartment of the cell a platinum sheet of size 15 × 20 × 2 mm was sealed to face the working electrode for impedance measurements. Anodic and cathodic polarization curves were traced at 1 mV s^{-1} scan rate. The impedance diagrams were recorded using an excitation AC signal of 10 mV peak to peak in the frequency domain 100 kHz down to 0.1 Hz. The measuring instrument was an electrochemical workstation IM6e Zahner-electrik, GmbH, (Kronach, Germany) provided with Thales software for I/E and impedance data analyses.

Corrosion products in solution were determined by atomic absorption spectrophotometry using an Analyst 100 Winlab-Perkin Elmer instrument. The microstructure of the film was identified by the diffraction patterns obtained from a thin film PERT PRO X-ray diffractometer using a copper (K_α) target with a secondary monochromator at omega = 0.5°. Elemental film composition was analyzed using JEOL microscope equipped with Oxford Link EDX microanalysis hardware.

3 Results and discussion

3.1 Open circuit potential

The variation of OCP with time of mechanically polished AZ91D alloy was recorded over 120 min in each 0.1 M solution of H_3PO_4, NaH_2PO_4, Na_2HPO_4 or Na_3PO_4 having pH values of 1.8, 4.5, 9.1 and 11.8, respectively. These electrolytes were chosen in order to enable the tests to be carried out over a wide pH range without changing the nature and concentration of the anions present. The results indicate spontaneous passivation for the AZ91D surface as can be substantiated from the continuous drift of the OCP with time in the positive direction, quickly at first and then slowly. The time needed to reach a steady state potential (E_{st}) decreases with increase in solution pH amounting to 25−10 min. The value of E_{st} is pH-dependent and becomes less negative with increasing pH, as shown in Table 1. The results in general indicate that phosphate solution sustains the process of oxide film formation as a result of spontaneous oxidation of the surface via a dissolution-precipitation mechanism [11, 12], which is likely to occur at the early stage of electrode immersion.

Table 1 Open circuit steady potential (E_{st}) for AZ91D alloy measured after 2 h from immersion in 0.1 M of the relevant solution

Solution	E_{st} /V(SCE)
(a) H_3PO_4 (pH 1.8)	−1.702
(a) NaH_2PO_4 (pH 4.5)	−1.633
(b) pH 4.5	−1.545
(a) Na_2HPO_4 (pH 9.1)	−1.465
(b) pH 9.1	−1.354
(a) Na_3PO_4 (pH 11.8)	−1.429
(b) pH 11.8	−1.449

(a) 0.1 M phosphate-containing solution

(b) 0.1 M phosphate-free solution

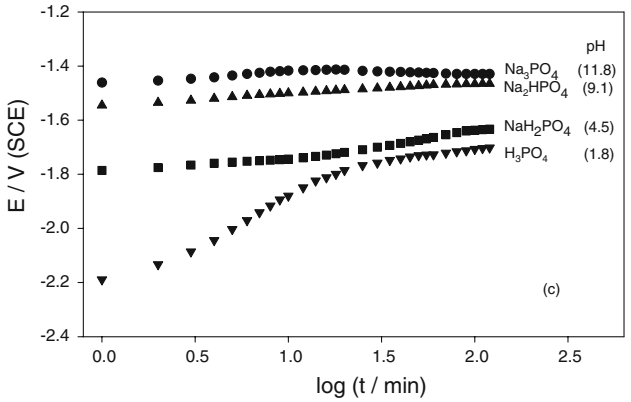

Fig. 1 The OCP versus log t plots for AZ91D alloy in 0.1 M phosphate solutions of various pH

By considering the variation of OCP(E) with the logarithm of time (log t) shown in Fig. 1, it can be concluded that film growth follows a direct logarithmic law (Eq. 1) for which the formation process is the rate-limiting step [13]:

$$E = \text{constant} + 2.303(\delta/B)\ \log\ t \qquad (1)$$

where δ is the rate of film thickening per time decade and $B = (zF/RT)\alpha\kappa$, α being the transfer coefficient and κ the width of the energy barrier traversed by the metal ion during film formation; all other symbols have their usual meanings. Each graph in Fig. 1 consists of two linear segments indicating that the passive film grows at two different rates. Thus, the film has a bi-layered structure [14]. The results reveal that the growth rate along the first segment is higher than that for the second assuming that the innermost layer of the surface film is of different microstructure than its outermost layer, as discussed later.

Data in Table 1 clearly show that although E in Na_3PO_4 solution of pH 11.8 has a higher value than that in Na_2HPO_4 solution of pH 9.1, there is not such a large difference between the two values after 2 h. This trend can be attributed to the nature of the phosphate species

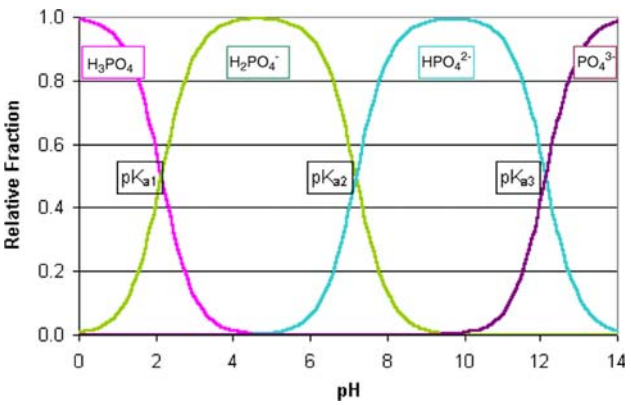

Fig. 2 Composition of the phosphate solution as a function of pH

prevailing at that pH (11.8). By analyzing the data in Fig. 2 [15] it is obvious that at pH 11.8, HPO_4^{2-} species has an almost equal tendency to exist in solution as PO_4^{3-} anions and thus the solution at this pH will contain the two phosphate species in nearly equal amounts.

It is of interest also to distinguish between the passivation behavior obtained in the phosphate containing solutions and that caused by pH increase in phosphate-free media. These measurements were established in solutions with similar pH values (4.5, 9.1 and 11.8) prepared by appropriate mixing of 0.1 M H_2SO_4 and 0.1 M NaOH solutions. At these three pH values the mean OCP results follow nearly the same trend, albeit with a different pH effect concerning the absolute E_{st} value (cf. Table 1). Thus, at pH 11.8 the E_{st} value lies nearly midway between those for PO_4^{3-} and HPO_4^{2-} solutions and at pH 4.5 E_{st} was found to be higher than that for $H_2PO_4^-$ medium, while at pH 9.1 it acquires its highest measured value. This implies that pH, as well as nature of the prevailing anions contribute to the spontaneous passivation of AZ91D alloy through possible incorporation of these anions into the lattice structure of the growing film [16], where they are located within the outer part of the passive film [13].

3.2 EIS measurements

The EIS characteristics of AZ91D alloy in 0.1 M solutions of H_3PO_4, NaH_2PO_4, Na_2HPO_4 and Na_3PO_4 corresponding to pH values of 1.8, 4.5, 9.1 and 11.8, respectively, were examined at the steady OCP after 2 h immersion, as shown in Fig. 3a, b. The Bode diagrams (Fig. 3a) show resistive regions at high and low frequencies and a capacitative region at the intermediate frequencies. This capacitive impedance is the least in H_3PO_4 solution of pH 1.8 and increases progressively with increasing pH, where it acquires its highest values in Na_3PO_4 solution of pH 11.8. Furthermore, two maximum phase lags appear at medium and low frequencies with the second having relatively smaller values and becoming undistinguishable as the pH decreases. The maximum phase angle (ϕ_{max}) at intermediate frequencies also increases with pH and gets broader in the following order $H_3PO_4 > NaH_2PO_4 > Na_2HPO_4 > Na_3PO_4$. Such behavior reflects an improvement in the insulating properties of the corrosion product layers on the alloy surface as the pH increases. The Nyquist plots (Fig. 3b) also reveal two scarcely capacitive loops merged into a large depressed semicircle at higher pH, indicating a very slow reaction.

Impedance response analysis was performed using the five-element RC electrical circuit (EC) drawn as an inset in Fig. 3a. This EC model used to fit the high and low frequency impedance data and involves two time constants R_1C_1 and R_2C_2 parallel combinations in series with the solution resistance (R_s). In this way C_1 is related to

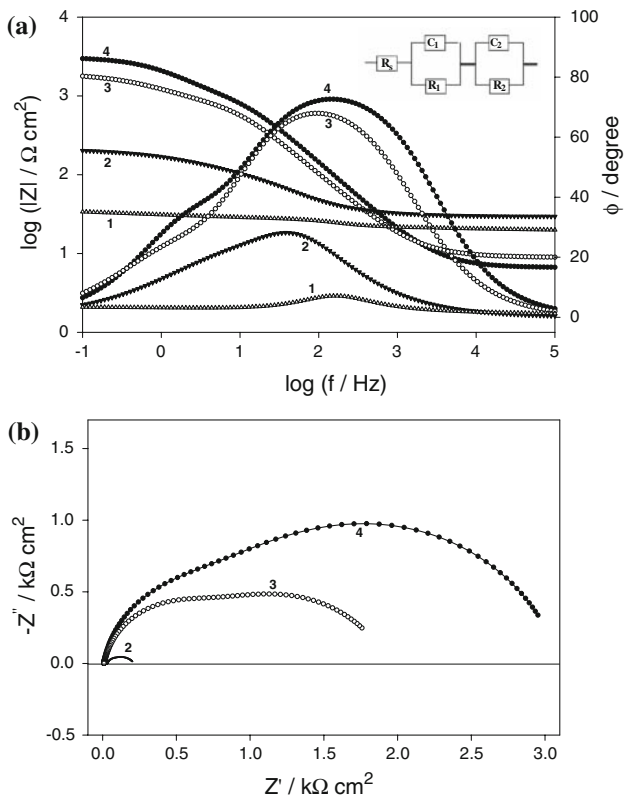

Fig. 3 Experimental and simulated electrochemical impedance data of AZ91D alloy immersed for 2 h in each 0.1 M solution of: (1) H_3PO_4 (pH 1.8); (2) NaH_2PO_4 (pH 4.5); (3) Na_2HPO_4 (pH 9.1); or (4) Na_3PO_4 (pH 11.8); (**a**) the Bode plots and (**b**) the Nyquist plots. Insert: equivalent circuit used for impedance data fitting

contributions from the capacitance of the outer layer and the faradaic reaction therein and C_2 pertains to the inner layer, while R_1 and R_2 are their respective resistances [17]. Two constant phase elements (CPE) are substituted for the capacitive elements C_1 and C_2 to give a more accurate agreement between measured and fitted data [18]. The CPE is a special element whose impedance is a function of the angular frequency ($\omega = 2\pi f$ rad s^{-1}) and related to that for a capacitor (C) as follows:

$$1/j\omega C = (1/Y_o)(j\omega)^{-\alpha} \quad (2)$$

where Y_o ($s^{\alpha}\ \Omega^{-1}$) is the frequency independent real part of the CPE, j is the imaginary root, α is an adjustable empirical exponent varies between 1.0 for a purely capacitive behavior associated with a perfectly smooth surface and 0.0 for a resistor. For real polished electrodes the value of α is less than 1.0, the lower the value the rougher the electrode [19]. Due to the heterogeneous microstructure of AZ91D alloy the corrosion product layer on the alloy surface has a heterogeneous structure. This heterogeneity increases the roughness of the electrode surface and decreases the value of α [20]. The above equivalent circuit was found to simulate the results and to give a better fit with an average error of about 5%.

The calculated equivalent circuit parameters are listed in Table 2. The results reveal that R_1 and R_2 increase with increasing pH, while C_1 and C_2 tend to decrease. This behavior indicates that spontaneously grown film on the alloy surface during exposure for 2 h is liable to dissolve in acidic solution more than in alkaline ones. According to the series model used in the analysis, the total film capacitance (C_T) is determined using the well known relation:

$$1/C_T = 1/C_1 + 1/C_2 \quad (3)$$

The passive film can be considered as dielectric plate capacitors formed between the metallic substrate and the counter electrode. Theoretically, film capacitance is related to film thickness (d) by the formula: $C_T = \varepsilon_o \varepsilon_r A/d$, where A is the film area, ε_o and ε_r are the dielectric constants of vacuum and film, respectively. Although the actual value of ε_r within the film is difficult to estimate, a change in C_T can be used as an indicator for change in the film thickness [13, 21, 22].

The effect of pH on the corrosion behavior is in agreement with the Pourbaix diagrams [23] of magnesium and aluminum. At open circuit conditions, Fig. 4 shows that the resistance ($R_T = R_1 + R_2$) of the film grown on AZ91D in phosphate electrolyte decreases with decrease in pH, exhibiting asymptotic behavior. The relative film thickness ($1/C_T$) follows almost the same trend, which indicates that thicker films are more passive than thinner ones. Overall, pH has a determinant influence on film properties; films formed in phosphate solutions at higher pH are thicker and afford better protection than those formed in acidic ones. Moreover, ϕ_{max} is the highest (73.4°) for AZ91D alloy immersed in basic Na_3PO_4 solution and decreases more rapidly with decreasing pH reaching only 7.7° in H_3PO_4

Table 2 Equivalent circuit parameters of AZ91D alloy immersed for 2 h in 0.1 M phosphate solutions of various pH values

Medium	R_s/Ω cm^2	R_1/Ω cm^2	C_1/μF cm^{-2}	α_1	R_2/Ω cm^2	C_2/μF cm^{-2}	α_2	R_T/Ω cm^2	$1/C_T$ /μF^{-1} cm^2	ϕ_{max}/degree
H_3PO_4 (pH 1.8)	18.3	33	41.60	0.37	4.0	283.0	0.908	37.0	0.030	7.7
NaH_2PO_4 (pH 4.5)	32.9	159	35.28	0.61	25.4	157.7	0.910	184.4	0.035	30.3
Na_2HPO_4 (pH 9.1)	8.9	1,326	24.70	0.73	600	19.80	0.926	1,926	0.091	68.2
Na_3PO_4 (pH 11.8)	6.6	2,446	18.60	0.82	652	15.35	0.934	3,098	0.120	73.4

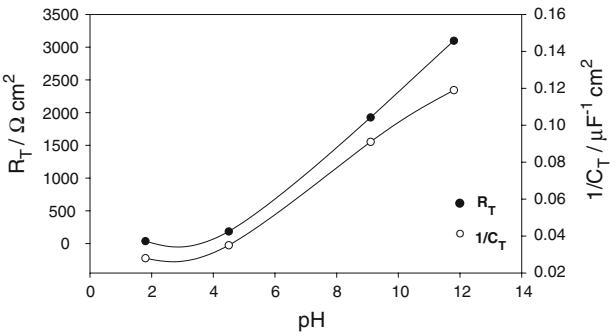

Fig. 4 The total resistance (R_T) and total relative thickness ($1/C_T$) for the surface film as a function of pH for AZ91D alloy immersed for 2 h in each 0.1 M solution of: H_3PO_4 (pH 1.8); NaH_2PO_4 (pH 4.5); Na_2HPO_4 (pH 9.1); or Na_3PO_4 (pH 11.8)

with simultaneous shift to higher frequencies indicating faster reaction at the lower pH. The behavior suggests better dielectric properties due to sealing of the surface by corrosion products as the forming pH increases.

It is well known that dissolution of magnesium in aqueous solutions proceeds by reduction of water molecules to produce magnesium oxide and/or hydroxide and hydrogen gas. Values of the cathodic Tafel plot β_c (given in Table 4) corroborate that the reduction process is primarily water reduction [24]. These reactions are insensitive to oxygen concentration [25], although the oxygen concentration is an important factor in atmospheric corrosion. Due to this hydrogen evolution, solution pH was found to rise at the end of the immersion test to 3.0, 6.2 and 10.2 for H_3PO_4, NaH_2PO_4 and Na_2HPO_4, respectively, while for the more alkaline Na_3PO_4 solution no significant pH variation was observed owing to the high stability of the AZ91D native film in this appreciably basic medium (pH 11.8).

Atomic absorption spectrophotometry (AAS) was conducted to determine the major alloy constituents that might enter the liquid phase at the end of 2 h immersion in 0.1 M H_3PO_4. The concentrations of Mg, Al and Zn in the test solution are, 61.75, 12.46 and 1.022 ppm (mg l^{-1}), respectively which reflects the composition ratios of the α-eutectic having higher Al content than the primary α phase. In the acidic phosphate medium, the microconstituent elements of the α eutectic are all more active than the β phase particles ($Mg_{17}Al_{12}$) over which the α eutectic precipitates [4, 26]. As a consequence this eutectic phase suffers galvanic corrosion. The probable overall corrosion reaction for AZ91D magnesium alloy is:

Anodic reactions

$$Mg + 2OH^- = Mg(OH)_2 + 2e \text{ (alkaline solution)} \quad (4a)$$

also,

$$\left.\begin{aligned} Mg &= Mg^{2+} + 2e \\ Mg^{2+} + H_2O &= MgO + 2H^+ \\ Al &= Al^{3+} + 3e \end{aligned}\right\} \text{ (acid solution)} \quad (4b)$$

Cathodic reactions

$$2H_2O + 2e = 2OH^- + H_2 \text{ (alkaline solution)} \quad (5a)$$

$$2H^+ + 2e = H_2 \text{ (acid solution)} \quad (5b)$$

Due to the high reactivity of AZ91D alloy in acid medium, hydrogen gas is also produced directly through the following step:

Chemical reaction

$$Mg + H_2O \xrightarrow{H^+} MgO + H_2 \quad (6)$$

The equilibrium pH value required for the precipitation of $Mg(OH)_2$ is around 11.0 [23], which means that alkaline phosphate solutions such as Na_2HPO_4 (pH 8.1) and Na_3PO_4 (pH 11.8), favour the direct precipitation of $Mg(OH)_2$ over the other two acidic solutions NaH_2PO_4 (pH 4.5) and H_3PO_4 (pH 1.8). Therefore, decrease in pH increases the corrosion kinetics and the alloy degradation proceeds at much higher rate, as indicated by the significant reduction in the values of both R_T and $1/C_T$, shown in Fig. 4. The corrosion process is mainly controlled by the oxidation products grown on the alloy surface. The thickness and propensity for hydration of the oxide was reported [27] to be reduced with increasing aluminum content (>4% which corresponds to ~35% Al in the innermost layer) and correspondingly, the oxide stability is increased. However, the present EIS results indicate that the protective properties and thickness of the surface film on the alloy are strongly pH-dependent where they both decrease significantly as the pH decreases following the sequence: $Na_3PO_4 > Na_2HPO_4 > NaH_2PO_4 > H_3PO_4$ (very low). In these solutions the OCP results (cf. Fig. 1) are in agreement with the two-time constant model shown as inset in Fig. 3a, which assumes a two-layer passive film structure at all pH values. Similar results were reported by Baril et al. [14], who found that for AZ91D alloy the film consists of an inner globular layer of MgO ~1.0 μm thick with an amorphous thicker porous outermost layer. Incorporation of electrolyte anions into the outermost layer [28] is beneficial from a corrosion point of view, since it significantly reduces porosity and reduces metal dissolution. This leads to an increase in R_1 of the outermost layer in comparison with R_2 for the innermost layer, as found experimentally (Table 2).

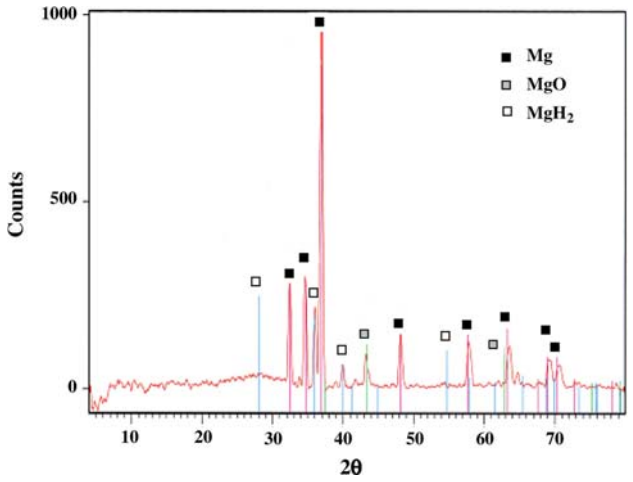

Fig. 5 Thin film X-ray diffraction spectrum of AZ91D alloy after immersion for 2 h in 0.1 M H_3PO_4 (pH 1.8)

3.3 Surface examination

Simple visual observations showed that as soon as the alloy sample was immersed in H_3PO_4 or NaH_2PO_4 solution, rapid violent reaction accompanied by gas evolution occurred. A concomitant deep grey-black layer formed on the alloy surface which became more evident with time, meanwhile gas evolution slowed down. On the other hand, for AZ91D sample exposed to Na_3PO_4 solution, no appreciable change in its surface was observed at the end of 2 h. Thus pH is a crucial factor in determining the nature and composition of the growing film.

The phase composition of the film formed on the alloy sample in acidic phosphate solution was analyzed by XRD and the result is presented in Fig. 5. The film consists mainly of crystalline hexagonal Mg (39%), cubic MgO (9.0%) and tetragonal MgH_2 (12%). Concerning the Pourbaix E-pH diagram for the Mg/H_2O system [23], shown in Fig. 6, it is clear that the whole domain of magnesium stability is well below that of water in neutral and low pH solutions. Therefore, magnesium dissolves as Mg^+ and Mg^{2+} accompanied by hydrogen evolution. Perrault [29] considered the formation of MgH_2 as well as Mg^+ and claimed, from calculation of the complete E-pH diagram of the Mg/H_2O system that thermodynamic equilibrium cannot exist for a magnesium electrode. However, such equilibrium is possible if the hydrogen overpotential has a value of about 1 V and the pH is above 5. Nevertheless, for AZ91D alloy in 0.1 M solution of H_3PO_4 or NaH_2PO_4, the results indicate that in a negative potential region <-1.6 V (SCE) the high rate of hydrogen evolution during the corrosion process leads to the formation of grey magnesium hydride (MgH_2) as a stable phase via the following electrochemical (9a) or chemical (9b) reactions [29]:

$$\left.\begin{aligned} Mg^{2+} + H_2 + 2e &= MgH_2 \\ Mg^{+} + H_2 + e &= MgH_2 \end{aligned}\right\} \quad (7a)$$

or

$$Mg + H_2 = MgH_2 \quad (\Delta G_f^o = -34.18\,\mathrm{kJmol^{-1}}) \quad (7b)$$

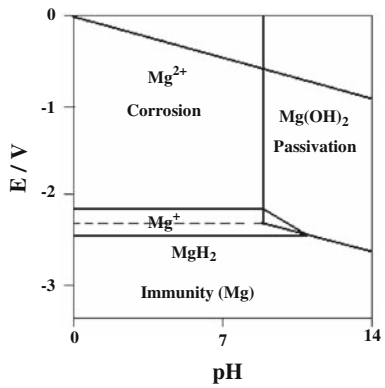

Fig. 6 Equilibria in the Mg-H_2O system in presence of H_2 molecules, at 298 K

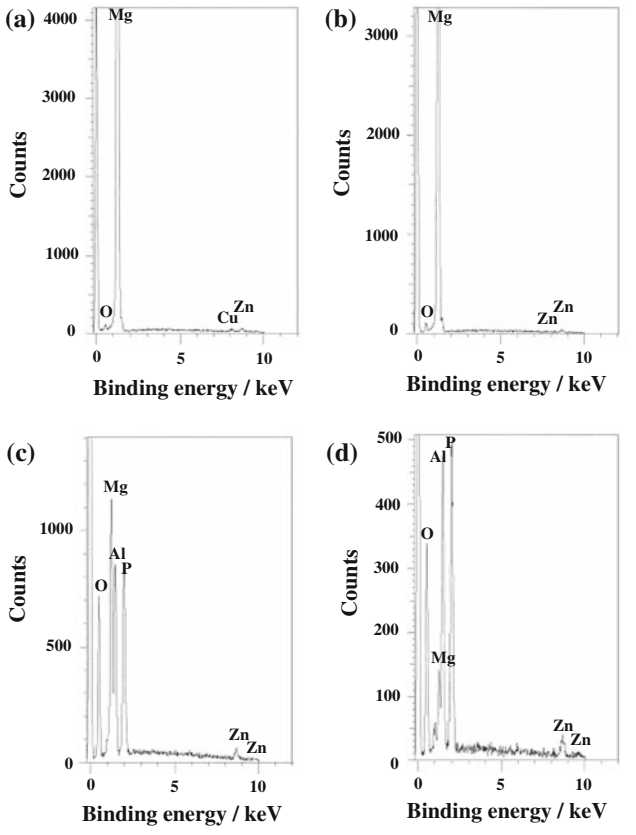

Fig. 7 (**a**–**d**) EDX spectra of AZ91D alloy (**a**) air exposed unimmersed sample (blank); and after immersion for 2 h in: (**b**) 0.1 M Na_3PO_4 (pH 11.8); (**c**) 0.1 M NaH_2PO_4 (pH 4.5); or (**d**) 0.1 M H_3PO_4 (pH 1.8)

Table 3 EDX elemental analysis data of the surface film formed on AZ91D in air or after 2 h immersion in 0.1 M phosphate solutions of various pH

Formation condition	Element						Relative stability (%)
	Mg (%)	Al (%)	Zn (%)	O (%)	P (%)	Cu (%)	
Air formed (blank)	99.2	–	0.3	0.3	–	0.2	100
Na_3PO_4 pH 11.8	98.7	–	0.2	0.2	–	–	99.5
NaH_2PO_4 pH 4.5	28.0	14.4	1.5	26.2	30.0	–	28.2
H_3PO_4 pH 1.8	5.30	19.8	1.5	29.6	43.8	–	5.3

Moreover, EDX spectra were used to determine the elemental analysis of the electrode surface before and after the immersion tests which give further evidence for the above results. Figure 7 presents EDX data for mechanically polished AZ91D air exposed sample and three other samples each exposed for 2 h to 0.1 M solutions of each Na_3PO_4, NaH_2PO_4 or H_3PO_4. For the unimmersed sample, the EDX spectra (Fig. 7a) show the characteristic peaks of some of the constituent elements. The EDX spectra for the Na_3PO_4 treated sample do not exhibit additional lines but only some enhancement in the oxygen signal and little reduction in the magnesium one (Fig. 7b). The stability of the air-formed film in this basic solution is thought to cause spontaneous passivation by reducing the charge transfer kinetics of water and/or oxygen reduction. For a sample treated in 0.1 M NaH_2PO_4 solution (Fig. 7c), however, the oxygen signal increases significantly while the magnesium main peak decreases, in addition to the appearance of two new prominent signals with high intensity corresponding to aluminium and phosphorous. The same spectra are also observed for the sample immersed in 0.1 M H_3PO_4 solution (Fig. 7d), but with more enhancement in the O, Al and P signals and greater reduction in the Mg peak.

The above data clearly demonstrate that a defective porous MgO film is formed in the aggressive acidic H_3PO_4 solution, as well as in the slightly acidic NaH_2PO_4 medium. Due to high porosity of the formed film, a large amount of phosphate ions from the electrolyte incorporates into its outer part [30]. In addition, EDX spectra indicate that following 2 h immersion in the appreciably basic 0.1 M Na_3PO_4 solution, the film formed on the surface is likely of similar nature as the pre-existing naturally air formed film which is highly stable and offers considerable protection to the alloy. Due to the galvanic effect between the primary α and the Al-rich β phase precipitated along grain boundaries and the presence of α-eutectic, the corrosion begins in the grain body then spreads to the eutectic areas. This leads to a strong aluminum enrichment of the corrosion product layer [31, 32], thereby its signal becomes visible in the EDX spectra (Fig. 7c, d). It is well known that the β phase ($Mg_{17}Al_{12}$) exhibits a passive behavior over a wide pH range than either of its components [33]. Song et al. [34] showed that the β phase can act as a galvanic cathode or as a barrier for anodic dissolution depending on its volume fraction on the surface. Hence, the relatively fine β phase network and the Al-enrichment produced on the corroded surface will be the key factors limiting progression of the corrosion attack.

Table 3 gives the EDX elemental analysis data for the air formed film and the films formed after 2 h exposure in 0.1 M phosphate solutions of various pH. Based on the at% Mg retaining in the surface film, which remarkably decreases with decreasing solution pH, the relative surface stability was calculated. This parameter represents the percentage ratio of Mg content in the surface film of the immersed sample to that of the air formed film. This seems a better way to describe the relative surface protection at various pH. It is clear that, in highly acidic solution, severe corrosion attack occurs and the corrosion product film affords inferior protection as compared to those formed at higher pH values.

3.4 Potentiodynamic measurements

Figure 8 shows typical linear cathodic and anodic polarization scans of AZ91D alloy in 0.1 M phosphate solution of various pH. Basically, in all solutions the alloy exhibits the same curve shape similar to that reported recently [22], where the current changes smoothly and linearly around the alloy reversible potential exhibiting cathodic and anodic Tafel behavior. Meanwhile, no active–passive transition peak can be discerned in the anodic trace, but a passivation plateau extending to a large domain of potential is observed characterized by an almost constant current density whose value increases monotonically with decreasing pH. Moreover, passive film breakdown is seen to occur at potential located above the reversible potential of oxygen evolution and is shifted to more positive values with increasing pH.

The main electrochemical parameters are presented in Table 4 and all are strongly pH-dependent. The results reveal that anodic and cathodic Tafel slopes (β_a and β_c)

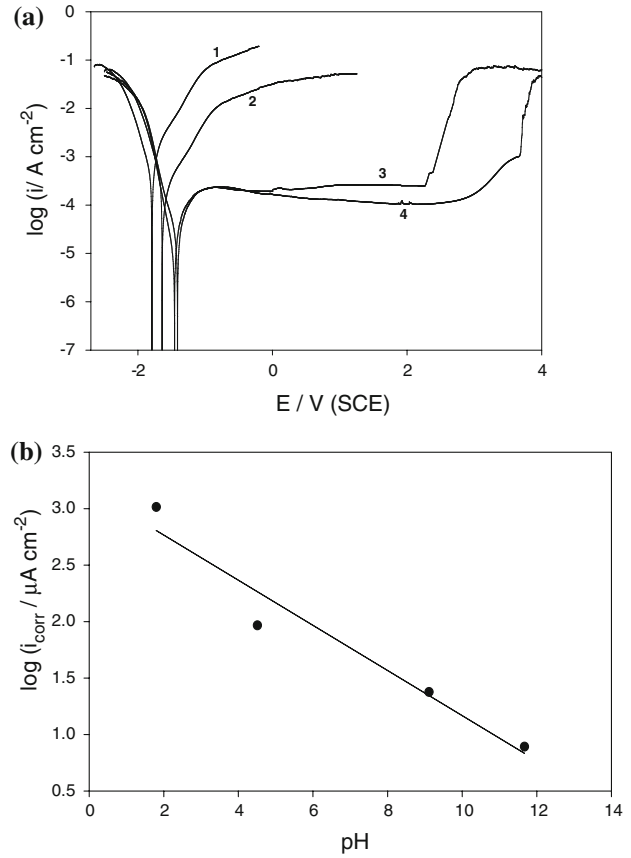

Fig. 8 **a** Potentiodynamic cathodic and anodic polarization scans of AZ91D alloy in each 0.1 M solution of: (1) H_3PO_4 (pH 1.8); (2) NaH_2PO_4 (pH 4.5); (3) Na_2HPO_4 (pH 9.1) or (4) Na_3PO_4 (pH 11.8). **b** Dependence of the corrosion current density (i_{corr}) of AZ91D alloy on pH of the phosphate solution

increase with decreasing solution pH which reflects more promotion in the anodic and cathodic partial reactions of the corrosion process represented by Eqs. 4 and 5, respectively. The corrosion potential (E_{corr}) and corrosion current density (i_{corr}) were calculated from the intersection of the anodic and cathodic Tafel lines extrapolation using Thales software. The E_{corr} values determined here are somewhat different from E_{st} values given in Table 1 from the OCP measurements. Indeed, this is due to partial removal of the passive film as polarization scanning was started at more negative potential relative to E_{st} value. On the other hand, the corrosion rate in terms of i_{corr} decreases almost linearly with increase in pH, as shown in Fig. 8b, following the relation:

$$\log i_{corr} = a - b\ \mathrm{pH} \tag{8}$$

where a and b are two empirical constants dependent on the examined system.

It is evident that, the corrosion rate in H_3PO_4 is the highest among the four tested solutions and decreases with increasing pH to become 100 times less in Na_3PO_4 medium. This means that AZ91D alloy has a very small corrosion resistance in H_3PO_4 solution of lower pH (1.8) and displays a superior anticorrosion performance in Na_3PO_4 solution of higher pH (11.8). Generally, the polarization results are in agreement with those obtained from EIS, and suggest that the quality of the spontaneously formed film, as a protective layer against corrosion, improves greatly at higher pH. This is probably due to the gradual conversion of MgO to the stable $Mg(OH)_2$, which leads to partial blocking of the film pores. Also, it has to be noted that in Na_2HPO_4 solution with pH 9.1, there was a visible white sludge deposit separated on the periphery of the electrode surface, which is likely to be due to precipitation of the insoluble $MgHPO_4$ as previously reported [10].

Table 4 Electrochemical corrosion parameters of AZ91D alloy immersed for 2 h in 0.1 M solution of each: H_3PO_4, NaH_2PO_4, Na_2HPO_4 and Na_3PO_4 of various pH

Medium	β_c/mV dec^{-1}	β_a/mV dec^{-1}	i_{corr}/µA cm^{-2}	E_{corr}/V
H_3PO_4 (pH 1.8)	−273	321	1,035	−1.79
NaH_2PO_4 (pH 4.5)	−237	266	92.5	−1.65
Na_2HPO_4 (pH 9.1)	−222	260	23.8	−1.47
Na_3PO_4 (pH 11.8)	−138	107	7.8	−1.43

4 Conclusion

The electrochemical techniques used in this investigation show that AZ91D alloy exhibits spontaneous passivation in 0.1 M phosphate solutions with various pH. This is evident by tracking the continuous positive shift in the OCP with both the immersion time and solution pH. Fitting the EIS data to a two-time constant equivalent circuit indicates that the film formed on the alloy is a bi-layered consisting of an innermost layer and a thicker outermost porous layer. Inclusion of phosphate species into the outer layer of the passivating film is responsible for the increase in its resistance (R_1) as compared with R_2 for the inner layer. Thin film XRD pattern reveals that the film formed in acid phosphate medium following 2 h immersion consists mainly of crystalline Mg, MgH_2 and MgO. The surface film stability significantly decreases in the order: $Na_3PO_4 > Na_2HPO_4 > NaH_2PO_4 > H_3PO_4$, which is the same sequence for increasing the corrosion rate of the alloy with increasing pH. It is assumed that spontaneously formed protective layers on the AZ91D surface greatly improve with increasing phosphate pH due to gradual conversion of MgO to $Mg(OH)_2$, which leads to partial blocking of the film pores.

References

1. Ghali E, Dietzel W, Kainer KU (2004) J Mater Eng Perfor 13:7
2. Ghali E (2000) Magnesium and Magnesium alloys. In: Revie RW (ed) Uhlig corrosion handbook. Wiley, New York
3. Avedesian MM, Baker H (1999) Magnesium and magnesium alloys, ASM speciality handbook. ASM International
4. Chen J, Wang J, Han E, Dong J, Ke W (2005) J Mater Corros 57:789
5. Polmear IJ (1995) Light alloys: metallurgy of the light metals, 3rd edn. Butterworth, Heinemann, Oxford
6. Li GY, Lian JS, Niu LY, Jiang ZH, Jiang Q (2006) Surf Coat Technol 201:1814
7. Hsiao H, Tsai W (2005) Surf Coat Technol 190:299
8. Zhou W, Shan D, Han E-H, Ke W (2008) Corros Sci 50:329
9. Zhao M, Wu S, Luo J, Fukuda Y, Nakae H (2006) Surf Coat Technol 200:5407
10. Niu LY, Jiang ZH, Li GY, Gu CD, Lian JS (2006) Surf Coat Technol 200:3021
11. De Pauli CP, Giordano MC, Lopez BA, Manzur E (1988) Corros Sci 28:769
12. Ismail KM, Virtanen S (2007) Electrochem Solid-State Lett 10:C9
13. El-Taib Heakal F, Ghoneim AA, Fekry AM (2007) J Appl Electrochem 37:405
14. Baril G, Blanc C, Pébère N (2001) J Electrochem Soc 148:B489
15. Bialkowski SE, http://www.chem.usu.edu/~sbialkow/Classes/3600/Overheads/H3A/H3A.html
16. Melendres CA, Camillone A, Tipton T (1989) Electrochim Acta 34:281
17. Chen J, Wang J, Han E, Dong J, Ke W (2007) Electrochim Acta 52:3299
18. Macdonald JR (ed) (1987) Impedance spectroscopy: emphasizing solid materials. Wiley, New York
19. Leibig M, Halseg T (1993) Electrochim Acta 38:1985
20. Benederti AV, Symodjo PTA, Nobe K, Cabot PL, Proud WG (1995) Electrochim Acta 40:2657
21. El-Taib Heakal F, Fekry AM, Ghoneim AA (2008) Corros Sci 50:1618
22. Zhang LJ, Fan JJ, Zhang Z, Cao FH, Zhang JQ, Cao CN (2007) Electrochim Acta 52:5325
23. Pourbaix M (1974) Atlas of electrochemical equilibria in aqueous solutions. NACE International, Houston, p 139 and p 168
24. Ambat R, Aung NN, Zhou W (2000) J Appl Electrochem 30:865
25. Uhlig HH, Winston R (1985) Corrosion and corrosion control. Wiley, New York (Chap. 20)
26. Chen J, Wang J, Han E, Ke W (2007) Corrosion 63:661
27. Nordlien JH, Nisancioglu K, Ono S, Masuko N (1996) J Electrochem Soc 143:2564
28. Hawke DL, Hillis JE, Pekguleryuz M, Nakatsugawa I (1999) In: Avedesian MM, Baker H (eds) Magnesium and magnesium alloys. ASM International, Materials Park, OH, p 194
29. Perrault GG (1974) J Electroanal Chem 51:107
30. Hubschmid C, Landolt D, Mathieu HJ (1995) Fresenius J Anal Chem 353:234
31. Baril G, Blanc C, Keddam M, Pébère N (2003) J Electrochem Soc 150:B488
32. Ballerini G, Bardi U, Bignucolo R, Ceraolo G (2005) Corros Sci 47:2173
33. Lunder O, Lein JE, Aune TK, Nisancioglu K (1989) Corrosion 45:741
34. Song G, Atrens A, Dargusch M (1999) Corros Sci 41:249